Properties of the offshore Low Level Jet and rotor layer wind shear as measured by scanning Doppler lidar

Pichugina Y.L., Brewer W.A., Banta R.M., Choukulkar A., Clack C., Marquis M., McCarty B.J., Weickmann A.M., Sandberg S.P., Marchbanks R.D., and Hardesty R.M.

University of Colorado Boulder and Earth System Research Laboratory of the National Oceanic and Atmospheric Administration

KEYWORDS

Low Level Jet, wind shear, Doppler lidar, offshore wind energy, wind profiles, rotor equivalent wind speed

Correspondence

Yelena Pichugina, CSD3/ESRL/NOAA, 325 Broadway, Boulder, CO, 80305 USA.

E-mail: Yelena.Pichugina@noaa.gov

ABSTRACT

The atmospheric flow phenomenon known as the Low Level Jet (LLJ) is an important source of wind power production in the Great Plains. However, due to the lack of measurements with the precision and vertical resolution needed, particularly at rotor heights, it is not well-characterized or understood in offshore regions being considered for wind-farm development.

This is the author manuscript accepted for publication and has undergone full peer review but has not been through the copyediting, typesetting, pagination and proofreading process, which may lead to differences between this version and the Version of Record. Please cite this article as doi: 10.1002/we.2075

The present paper describes the properties of LLJs and wind shear through the rotor layer of a hypothetical wind turbine, as measured from a ship-borne Doppler lidar in the Gulf of Maine in July-August 2004.

LLJs, frequently observed below 600 m, were mostly during nighttime and transitional periods, but they were also were seen during some daytime hours. The presence of a LLJ significantly modified wind profiles producing vertical wind speed shear. When the wind shear was strong, the estimates of wind power based upon wind speeds measured at hub-height could have significant errors. Additionally, the inference of hub-height winds from near-surface measurements may introduce further error in the wind power estimate. The lidar dataset was used to investigate the uncertainty of the simplified power-law relation that is often employed in engineering approaches for the extrapolation of surface winds to higher elevations. The results show diurnal and spatial variations of the shear exponent empirically found from surface and hub-height measurements.

Finally, the discrepancies between wind power estimates using lidar-measured hub-height winds and rotor equivalent winds are discussed.

1. INTRODUCTION

Offshore wind power is an important potential source of renewable energy, but so far it has not been widely developed in U.S. coastal waters. One impediment to such development is the near lack of measured wind profiles offshore of sufficiently high resolution and precision. Because of the great cost involved in offshore wind-energy facility construction and operations it is important to have enough appropriate environmental data to avoid regions of abnormally weak wind resources or abnormally harsh meteorological and oceanographic conditions. It is crucial to have reliable data for

both wind resource-assessment purposes and to understand the wind-flow variability in space and time. Several studies have shown that Doppler lidars are able to fulfill this need by providing high-quality measurements of wind speed and turbulence profiles from the surface up to several hundred meters aloft.[1-4]

Some studies have placed lidar systems on the nacelle of offshore wind turbines to obtain information about inflow winds at various distances upstream of the turbine.[5] Another option is to use existing fixed offshore platforms for lidar deployment, but the location of these platforms may not be desirable. Lidars may also be mounted on transportable floating platforms, such as ships or buoys. However, significant technological obstacles are associated with compensation for ocean-wave-induced and other platform accelerations in calculating the derived lidar measurements of the airflow. In open ocean waters, motion compensating techniques are critical for obtaining reliable estimates of wind speed and direction from lidar measurements.

To obtain quantitative information about the wind flow in a marine environment, the present paper uses High Resolution Doppler Lidar (HRDL) measurements taken from a research ship in the Gulf of Maine. HRDL is a research scanning, pulsed Doppler lidar[6, 7] developed and operated by the Earth System Research Laboratory (ERSL) of the National Oceanic and Atmospheric Administration (NOAA). This lidar is equipped with a motion-compensating scanning system shown to be effective in overcoming measurement errors related to ocean and ship motions.[8] This lidar system was deployed on the *Research Vessel Ronald H. Brown* (*RHB*) during the New England Air Quality Study [9,10,11,12] over the summer of 2004 (NEAQS-04) to provide accurate profile data of wind speed and direction in the lowest several hundred meters of the marine boundary layer (MBL) with high temporal and vertical resolutions. These high-quality measurements provide valuable information about the environment in which the turbines will be operating—in the layer of atmosphere most critical for wind energy. Samples of these measurements were used in Pichugina et al.[8] to analyze the vertical-,

horizontal-, and time-evolving structure of MBL wind profiles and to investigate the departures of measured wind-profile shapes from their corresponding power-law profiles in certain case studies.

In the present paper we broaden the investigation by using the entire data set, but with a focus on quantifying offshore LLJ properties observed during NEAQS-04; including frequency, strength, height of the jet maxima, the magnitude of the shear within the rotor layer, and contributions to uncertainties in power determination.

The manuscript is organized as follows. Section 2 explains the calculation of wind speed and direction profiles from ship-borne lidar measurements of the radial velocity during conical scanning at shallow elevation angles. Section 2 also contains brief descriptions of wind and weather conditions during the NEAQS-04 experiment, along with assessments of the accuracy of the motion-compensated lidar measurements. Section 3 gives examples of LLJ events observed during case studies. It also contains a discussion about distributions of LLJ characteristics, including wind speed maxima and heights of these maxima, over the duration of the experiment. Section 4 contains examples and time series of mean wind speed and direction at several heights and shows wind and directional shear across the rotor layer of a hypothetical wind turbine, having a hub-height at 100 m above the water surface and a rotor diameter of 100 m. In addition, we discuss the variations associated with LLJ occurrence in the extrapolation of near-surface measurements to hub-height by using the power-law relationship. The section shows that the diurnal and spatial variations of the power law shear exponent found empirically from the lidar measurements are large. Section 5 presents the uncertainty in power estimates between measured hub-height and rotor equivalent winds, discussing two different techniques to compute rotor equivalent winds[13, 14] and comparing wind-power estimates based on the lidar measured hub-height winds and the computed rotor equivalent winds.[13] Finally, Section 6 summarizes key results from this study.

1.1 Background

Low Level Jets (LLJs) are well known phenomena over flat terrain in the Great Plains. [15,16,17,18] In a nocturnal stable boundary layer, winds at higher levels accelerate relative to the surface winds creating a LLJ, which is characterized by a wind profile with a distinct wind maximum and generally reduced wind speed above and below that maximum.[18,20] Such profiles were frequently observed in HRDL measurements during the CASES-99 and Lamar-03 field campaigns.[18,20] The wind speed maximum was generally seen at 90-250 m (within or just above the rotor layer) along with strong wind shear. The intense shear within the rotor layer is responsible for the formation of turbulent motions that may generate excessive vibration in turbine parts.[21]

In contrast to Great Plains LLJs that have been mostly attributed to inertial oscillations[15], offshore LLJs observed in different coastal regions are often attributed to baroclinic effects associated with land–sea temperature gradients.[22, 23] Thermal wind processes associated with land–sea heating contrasts have been identified as fundamental to occurrence of these LLJs.[24] Topography also plays a role in providing local wind enhancements near coastal zones.[25]

In the summer time LLJs were frequently observed along the west coast of the United States approximately at 300–400 m above sea level.[26] LLJs were also reported as a common feature of a shallow stable boundary layer in summer from wind profiling radar data[9] and from case studies of lidar-measured wind profiles over the cool waters of the East coast.[8] These jets were observed at, or slightly above, the common heights of wind turbine rotors, creating shear through the rotor layer that may influence wind turbine operations. Recent offshore measurements taken with the SgurrEnergy Galion lidar on a wind farm in the North Sea showed that offshore LLJs may also increase loads on wind turbines and therefore increase component failure rates.[27]

2. SHIP-BORNE LIDAR MEASUREMENTS

The HRDL deployed on-board the ship captures high-precision and high-resolution measurements of radial velocity, while compensating for ocean and ship motion. The achieved pointing angle accuracy of the laser beam was 0.1° for static precision and less than 0.5° for dynamic precision. A more detailed description of HRDL's technical parameters and motion compensating system is provided in Pichugina et al.[8]

Wind speed and wind direction profiles

In the present study, the HRDL dataset is used to analyze LLJ and wind shear properties. The dataset consists of HRDL scan data taken in recurring 15-min scan sequences, which have been analyzed into 15-min averaged profiles of wind speed and direction. These profiles were obtained from radial-velocity measurements from conical scans at several (0°, 2°, 5°, 10°, 15°, and 30°) elevation angles. The technique used was a modified velocity-azimuth-display (VAD) analysis procedure—a modified form of the VAD technique using all of the conical scans that were performed at multiple elevation angles in each 15-min scan-sequence averaging interval, to form a single mean profile.[28, 29, 50.] Profile data at 15-min were used because of the way the data were taken, but the behavior of the winds in time and space and the conclusions drawn would apply equally to 10-min profiles used commonly in the wind industry.

A Google-Earth map of the study area, which has the ship tracks during the entire experiment, is shown in Fig. 1. Each circle represents the location (latitude and longitude) of 15-min averaged wind profiles from near surface up to ~2.5 km. The vertical resolution of these profiles is approximately 10-15 m, denser in the first 200 m[50], which is the region of most interest to this study.

In total, approximately 2,000 of the 15-min averaged profiles were analyzed to indicate LLJ strength, height of jet maxima, and wind shear across the rotor layer of 50-150 m, for the hypothetical wind turbine.

Wind and weather conditions during the NEAQS-04 experiment

Profiles were obtained from the entire 2004 field campaign that took place between July 09 and August 12. During some short periods, meteorological conditions prevented the lidar from operating. Thus lidar data were unavailable on July 15, 19, and August 2 due to heavy rain. On a few other days, the data were obtained for limited time periods (less than 6 hours), due to heavy rain or dense fog. On July 24 the *RHB* was in port for a scientific meeting. In general, wind speeds within the rotor layer over the entire experiment were moderate (<12 m s^{-1}), and stronger at night, due to LLJ activity. Several episodes of strong wind speeds (>15 m s^{-1}) were observed (specifically on July 16, 31, and August 11-12). In a few cases (July 10, 21, and August 7) wind speeds dropped to less than 2 m s^{-1}. Overall; the mean wind speed within the rotor layer was 7.2 m s^{-1}, and the median value was 6.6 m s^{-1}. The prevailing wind direction was south/south-westerly with a mean value of 216°.

The accuracy of lidar-measured wind profiles

Significant technological obstacles to obtaining accurate wind profiles offshore are associated with the removal of ocean-wave-induced and other platform accelerations from the desired measurements of the airflow. The motion-compensation system employed during the NEAQS-04 experiment has been evaluated in several ways, and the accuracy of the lidar-measured wind profiles was assessed by comparison with profiles measured by other instruments operated from the ship[8-12, 30]. Pichugina et al.[8] compared HRDL measurements at 12.9 m above the ocean surface with in-situ sonic-anemometer ‘‘flux-wind’’ measurements[10] at a height of 17 m protruding from the bow of

the ship and also compensated for the motions of the ship. They found good agreement, with correlation coefficients of 0.92 for wind speed and 0.98 for wind direction. Another validation of the HRDL measurements from the ship was reported in Wolfe et al.[11] using measurements from radiosondes released from the deck of the ship every 6 hours for a total of ~120 soundings. Horizontal and lateral wind components from both instruments show good agreement with correlation coefficients of 0.97 and 0.98, respectively.

These results were found for wind speed values averaged over all heights above 100 m. In Fig. 2, we compare HRDL and radiosonde profile data at each individual height to assess measurement differences through the rotor layer. Profiles of correlation coefficient are shown in the left panel of the Fig. 2. The right panel shows the number of points used for each comparison height from the surface to 1500 m. Reduced correlation coefficients (less than 0.96) were found at the three lowest heights of 30, 60, 90 m, indicating the influence of the ship's atmospheric wake on the radiosonde's measurements at these levels.[8]

Since the motion-compensated HRDL measurements are accurate and have high spatial and temporal resolution, they are an appropriate choice to statistically characterize LLJ properties including frequency of occurrence, jet speed maxima, and the height of these maxima, and to investigate shear through the rotor layer.

3. LOW-LEVEL JET

We analyze LLJ behavior within the lowest kilometer of the marine atmosphere. A time-height cross section showing an example of the LLJ diurnal evolution on August 11 is shown in Fig. 3, which shows jets exceeding 15 ms^{-1} observed during 0-15 UTC, and again during 21-22 UTC, when the *RHB* was farther out to sea[8]. LLJ structure above and below the jet maximum was evident in more than half of the 15-min averaged wind

speed profiles from this sampling period as illustrated in Fig. 4, where only even hours are shown. To identify the LLJ we used criteria[18,19] that allow the detection of jet structure below 1 km as demonstrated in Fig. 4.

Statistical analysis of the 15-min wind profiles from HRDL measurements over the entire experiment reveals occurrences and mean values of LLJ characteristics. From HRDL measurements we identified 1,247 (~63%) wind profiles that contained LLJs. Figure 5 shows the distribution of the LLJ speed maxima (U_J) and the distribution of the heights of these maxima (Z_J). U_J varied from 5 to 20 m s^{-1} with a mean value of 9.4 m s^{-1} and median of 8.7 m s^{-1}. The majority of LLJs observed had wind maxima less than the turbine rated wind speed of 12 m s^{-1}, where power generation is most sensitive to changes in wind speed, although occasional stronger jets did occur. In most cases, the height of the U_J was found below 200 m, although occurrences of jets at higher altitudes are present. The mean value of the Z_J distribution was 149.3 m, and the median, 124.7 m. Such results cannot be captured by surface measurements or by remote sensing instrumentation having coarser vertical resolution (e.g., 50-100 m range gates).

Over land, LLJs (often nocturnal in nature) occur in many parts of the world[31], including the U.S. Great Plains, where studies using Doppler lidar have been able to document their detailed structure and characteristics[3,18,32,33]. Similar to the nocturnal LLJ over the Great Plains[18], stronger offshore jets during NEAQS-04 tended to be higher, extending up to 600 m as indicated in Fig. 6a by black symbols. Several occasions were found, however, when jet maxima were located close to hub-height, as indicated by color symbols for days according to the legend. An example of one of these days, when strong (>15 m s^{-1}) LLJs were located near hub height, is illustrated in Fig. 6b and 6c for July 31.

The spatial distributions of LLJ speed and height are shown in Fig. 7a and b. Both strong and weak jets can be seen at all locations over the Gulf of Maine, appearing to be independent of distance from shore or other geographic factors. Jet heights are

mostly less than 200 m ASL as shown in Fig. 5, but the higher LLJs in this dataset are only seen south of 43°N latitude. Thus the strong jets north of this latitude were low jets, indicating strong shear values in the sub-jet layer.

The frequency of LLJ occurrence described here was obtained from a one-month, summertime dataset of lidar measurements along ship tracks (Fig. 1). Analysis of seasonal wind regimes in the Gulf of Maine, using a 3-year (2012-2015) archive of forecasts from an experimental version of NOAA's High Resolution Rapid Refresh (HRRR) model, shows that offshore wind speeds reach a maximum during the winter months (Dec – Feb), and a minimum in the summer (Jun – Aug)[34,35]. Analysis of 10-year means from buoy observations in the experiment region (http://www.ndbc.noaa.gov/), as well as climatological analysis from literature[9], also show that mean surface wind speed in July and August in this region are the lowest for the year. Strong winds in fall, winter, and spring are expected as the result of traveling storm systems, but in summer the storm tracks are well to the north, and the occasional storm that does come through has weaker winds in general than cool-season storms (except, of course, for hurricanes). Thus, during the warm season, rotor-level winds driven by LLJs probably represent an important resource for wind energy.

4. ROTOR-LAYER SHEAR

As discussed in the previous section, the existence of LLJs may significantly modify the wind speed profile and create shear across the rotor-blade sweep area. Examples of wind profiles in Fig. 8 illustrate three different cases of shear through the rotor layer. Jet maxima at the top of (or above) a rotor layer cause a positive wind shear across this layer (Fig. 8a), whereas wind maxima in the bottom part of (or below) this layer cause negative shear (Fig. 8b). For the case when the jet nose is near hub height (Fig. 8c) the calculated *net* shear across the rotor layer may be small, but rotor blades would

experience wind-speed maxima (when horizontal) and minima (when vertical) twice during a full 360° rotation and potentially significant shears across both the top and bottom halves of the rotor disk. Examples given here were for periods when LLJ maxima were less than 7-8 m s^{-1}. For stronger wind cases (as in Fig.4, wind profile at 1400 UTC), shear and shear-generated turbulence may be strong enough to produce additional stresses on turbine parts, reducing their lifetimes and overall energy-production performance.

Figure 9 shows diurnal variations of the (a) wind speed, (b) wind direction, (c) speed shear and (d) directional shear, averaged over the entire experiment (July 9-August 12). Significant diurnal variations of hub-height winds have been observed during individual days of strong winds[8]. However, experiment-mean fluctuations of winds are relatively smaller. Values of minima, maxima, mean, and standard deviations of wind speed, direction, wind and directional shear are shown in Table 1.

In the presence of LLJs, enhanced winds during evening/early morning hours (00-11 UTC, 1900-0600 local standard time) caused stronger rotor layer wind speed shear, so turbine blades would harvest stronger winds at the top and weaker winds at the bottom parts of this layer. In the mean, variations of wind direction, both in time and through the rotor layers, were relatively small, the difference between the top and the bottom of the rotor layer averaging 20° or less. Wind shear and veering for some individual days from the NEAQS experiment were significantly larger than these mean values[8].

WRF modeled winds during coastal low-level jets “show an extraordinary amount magnitudinal and directional vertical wind shear throughout depths common for wind turbine rotor planes (40-140 m AGL)”[36], however, as with all model-generated findings, these results need to be verified by measurements. The strong speed shears reported here are consistent with these model-based conclusions.

Overall offshore winds during the NEAQS-04 experiment during nighttime hours were weaker compared with winds that were observed by HRDL over flat terrain in the U.S. Great Plains. Values of rotor-layer wind shear were half as large (0.021 s^{-1}) as observed over flat terrain near Lamar, Colorado (0.048 s^{-1}) or Kansas (0.039 s^{-1}).[3, 8, 29] Note that larger shears of up to 0.10 s^{-1} have been routinely measured in the layer below the LLJ maxima over land.[32, 37]. The large Great-Plains shear values have been attributed primarily to the large degree of decoupling of the flow in the lowest few 100 m above the surface, due to the arid conditions, the strong surface cooling, and the resulting strong near-surface stability[33]. Such strong cooling, stability, and decoupling are not observed at the ocean surface.

a. Surface and hub-height winds

Measured profiles of the winds should be the preferred method for determining wind properties at hub height and through the rotor layer. But instrumentation is not routinely available to directly measure these winds, so in this case, one often relies on near-surface measurements and wind-profile extrapolation formulas, such as power law or logarithmic law relations, to calculate wind estimates aloft in the rotor layer. For example, in U.S. coastal areas, the most complete database of offshore wind speed and direction is provided by the NOAA National Weather Service's National Data Buoy Center network of sonic-anemometer measurements at 3-5 m above the water surface.

In the absence of reliable measurements at turbine-rotor height[38], the accuracy of these extrapolations is unknown[39,40], although it was shown that the shapes of individual HRDL-measured profiles over the Gulf of Maine seldom conform to those of standard profiles.[8] In particular, profiles such as in the middle and right panels of Fig.8, exhibiting negative shear or a LLJ nose within the rotor layer, cannot be represented by either of these profile shapes at all. Setting aside the question whether the power-law expression is appropriate, it is still widely used where direct hub-height measurements

are unavailable, so it is of interest to further investigate the range of magnitudes in using the power-law exponent α found over the Gulf of Maine, and whether wind-speed profiles having LLJ structure exhibit different α values.

Figure 10a shows the diurnal variations of lidar-measured winds at 10 m above the water surface and at 100 m, the assumed hub height, averaged over the entire period of July 09-August 12. During nighttime hours (02-10 UTC), the mean difference between the wind speeds at these two heights was more than 2.5 m s^{-1}, decreasing to 1 m s^{-1} during late afternoon hours (14-19 UTC). Wind speed at these two heights were used to calculate a measured empirical value for α for the wind conditions during NEAQS-04. The diurnally varying mean values for α associated with these wind speeds are shown in in Fig. 10b, where nighttime values (0.19) were 63% larger than the daytime values (0.12).

Wind speeds at 10 and 100 m were also differently distributed in the horizontal, as illustrated in Fig. 10c mostly due to the frequent occurrence of LLJ-shape profiles. The α values computed from all HRDL-profile measurements at 10 and 100 m varied over a wide range, between 0 and 0.6, as shown in Fig. 11a, where the mean and median values equaled 0.16 and 0.15, respectively. In this case, the spatial variability of α is shown in Fig. 11a1, where the values are color-coded from 0.0 to 0.5. Distance from shore did not appear to have a strong effect on the value of α.

The distributions of α values and their spatial variability for profiles having and not having LLJ structure are shown in Fig. 11b and 11c, respectively. The median value of α for the sample with LLJ structure was nearly 15% larger than the value for all profiles, and much larger (89%) than for the sample with no LLJ structure—not surprising, since the larger values of α reflect the larger shears when LLJs were present. The spatial distribution of the with-LLJ data points in Fig. 11b1 show again that LLJ occurrence was well distributed horizontally--near-shore LLJs were as likely as those far from shore--consistent with Fig. 7. The large values of the shear exponent in the northern part of the

area are a result of the low, strong jets noted previously in that region. As shown on Fig. 11c, the mean (0.12) and median (0.09) values of α computed for profiles with no LLJ structure are close to these often used in practice.

The usefulness of the power-law profile for vertical extrapolation of wind speeds depends completely on whether the proper value for α can be specified in advance for each location and time. The strong spatial and temporal variability of α over a limited region such as the Gulf of Maine shows that this is likely to be very difficult.

Overall, for statistically accurate conclusions on the meridional distributions of winds LLJs, and α more uniform offshore measurements are needed from a carefully planned experiment using several measurement platforms.

5. EQUIVALENT WIND SPEED

In the presence of the LLJ and strong shear through the layer of the atmosphere swept by large wind turbines offshore, the uncertainty in the power-curve estimates using point measurements at hub-height could be significant. A proposed concept of the "equivalent wind speed"[45] accounts for the wind shear and the turbulence intensity across the rotor layer. Under this concept the rotor equivalent wind speed (REWS) is computed by using wind speed measurements at several heights across the rotor layer (rather than just at hub height) and totaling these values, weighted by the segment area of the circle whose radius is equal to the length of turbine blades.

The effect of wind shear on the accuracy of wind power estimates was tested by Wagner et al.[13] using wind measurements at several heights across the turbine rotor layer obtained from two tall towers. The results of their study showed better estimates of the power production using the rotor equivalent wind speed compared to the wind speed measured only at hub-height.

In addition to wind shear, other factors may influence turbine operations and power generation including wind turbulence,[46] wind direction,[47, 48] and wind directional shear.

To assess the combined effects of all these factors, a new formulation of the rotor equivalent wind was presented by Choukulkar et al.[14] This concept accounts for the total impact of wind speed and directional shear, turbulence, and wind-direction fluctuations on the estimated power production. This technique was tested[14] using Doppler lidar measurements[4] of wind flow over flat terrain in the Great Plains and lidar measurements over semi-complex terrain in the vicinity of the Rocky Mountains.[49,50] It was shown that, in addition to wind speed shear, accounting for wind directional shear and direction fluctuations through the rotor layer can produce up to 1.3% difference, on average, in the estimated power production.[14]

In the present paper we compare hub-height and rotor-equivalent winds[14] computed from lidar measurements with high vertical resolution through the rotor layer. Hereafter we will indicate a wind speed measured at hub height as U_H and related wind power as P_H. We also will refer to the rotor equivalent wind speed and related power as U_{eq} and P_{eq} respectively. The equations used to estimate the REWS and rotor equivalent power are shown in Eqs. (1) and (2) respectively.

$$U_{eq} = \sqrt[3]{\frac{1}{A}\sum_{i=1}^{N}\overline{U}_i^3\left[1+3\left(\frac{\sigma_{ui}}{\overline{U}_i}\right)^2\right]\left[1-\frac{\overline{\varphi}_i^2}{2}-\frac{\sigma_{\varphi i}^2}{2}\right]^3 A_i} \quad (1)$$

$$\overline{P}_{eq} = \frac{1}{2}\rho C_P\sum_{i=1}^{N}\overline{U}_i^3\left(1+3\left(\frac{\sigma_{ui}}{\overline{U}_i}\right)^2\right)\left[1-\frac{\overline{\varphi}_i^2}{2}-\frac{\sigma_{\varphi i}^2}{2}\right]^3 A_i \quad (2)$$

where σ_{ui}^2 is the variance of velocity fluctuations at *i*-th level, φ_i is the angle of the wind with respect to the rotor axis at *i*-th level, $\overline{U}_i$ is the wind speed at the *i*-th level, $\sigma_{\varphi i}^2$ is the direction-fluctuation variance at the *i*-th level, and A_i is the area of the fraction of the swept area at the *i*-th level.

The REWS and rotor equivalent power for the entire measurement period were estimated using Eq. (1) and (2). For the purpose of these calculations, an Enercon E82 turbine is taken as an example in order to use a realistic C_P curve. Individual 15-minute REWS estimates vs. hub-height wind measurements show wind-speed differences varying between -2.38 m s^{-1} and 2.93 m s^{-1}, with the experiment mean value of 0.18 m s^{-1}. The resulting power differences varied between -0.67 MW and 0.42 with an experiment mean difference close to zero. Overall, the hub-height and the rotor equivalent wind speed and related power were highly correlated with R^2 of 0.99 for both variables.

To understand the ramifications of using the REWS formulations versus the hub-height values, the percentage difference in power production estimates using the hub-height wind and REWS is calculated and presented in Fig. 12. The top of this figure shows the normalized bias averaged over the measurement period as a function of time of day along with the ± standard deviation spread indicated by dotted lines. This normalized bias fluctuated over the diurnal cycle, showing differences up to 10% for some periods. However, individual differences (in 15-min average power estimates) could be as large as 30% during some periods. The bottom panel gives the root-mean square difference (RMSD) between the actual powers P_{eq} and P_H. The RMSD varied between 0.02 and 0.15 MW with an experiment mean error of 0.06 MW.

This analysis demonstrates that subtle differences in wind speed estimates (REWS vs. hub-height) can create variations of up to 30% in expected power. Obviously the numbers presented in this summertime study are not indicative of annual trends in expected power. Given the limited range of wind speeds encountered during this period, the variation in expected power over the full range of the wind turbine power curve was not characterized. Therefore, it is clear that measurements such as those presented in this paper need to be performed over extended periods to capture the full range of influence of the marine atmospheric boundary layer on expected wind turbine

performance. Overall, these results are in agreement with previous studies[13, 14, 51, 52] suggesting that the use of a single point measurement at hub-height would provide greater uncertainties for conditions of stronger winds and larger shear through the rotor layer.

6. SUMMARY

Existing lidar measurements from previous offshore measurement campaigns can provide valuable information on the profiles of marine wind-flow properties, especially considering the great expense of doing new field programs. A dataset obtained from ship-borne Doppler lidar measurements in the Gulf of Maine from 09 July to12 August 2004 was used to study Low Level Jet (LLJ) properties and shear through the layer of the turbine blade span area. A high frequency (about 63%) of LLJs was evident in the lidar-measured vertical wind-speed profiles below 600 m, especially during night and transitional periods, but also during daytime hours on occasion. The maximum of the jet speed varied from 5 to 20 m s^{-1} with mean value of 9.4 m s^{-1}. Maximum jet heights extended up to 600 m, with a mean value of 156.6 m.

The existence of LLJs significantly modified the wind profiles producing vertical wind shear of 0.03 s^{-1} or more across the assumed rotor layer of 50-150 m. LLJs also produced wind profile shapes that deviated significantly from the normal wind-profile shapes often used for extrapolation of surface measurements to turbine hub heights (e.g., the power-law profile). The value of the shear exponent α, empirically found from HRDL measurements near the surface and at hub height, showed strong spatial variability and diurnal variations from 0.1 to 0.25 with a mean value of 0.165 for the NEAQS-04 dataset.

The high vertical resolution of lidar allowed wind power estimates based on hub-height and rotor equivalent winds to be calculated and compared. Significant differences

were found for individual sub-hourly profiles. Differences were also found for longer-term averaging, which could amount to significant deviations in revenues generated.

The availability of accurate, high-resolution profile data gives a number of advantages in determining quantities of interest to wind energy.

As shown in this study, the lidar/motion-compensation system can be used to better understand the range of atmospheric conditions, and their spatial and temporal variability.

The existence of spatial variability in the offshore wind field has important consequences for wind energy. Regions of enhanced speeds, which may be tied to shoreline irregularities or coastal topography, would be favored for energy generation, whereas other regions of reduced winds may not. Obviously it is important to be able to identify the more favorable locations, but spatial variability also affects the ability to sample the flow field. Isolated in-situ or profiling instrumentation on a fixed mast or platform is incapable of detecting spatial variability, so the representativeness of such measurements is an issue. Arrays of fixed measurements can sample spatial variability, but the relevant spatial scales of variability must be known and factored into the array design. Scanning remote-sensing instrumentation can be used to determine scales smaller than the scan diameter. This paper has presented a sampling of the kind of information available from ship-borne lidar measurements. The results presented could not have been obtained from surface measurements alone or from remote sensing instrumentation with coarser vertical resolution and precision of data.

ACKNOWLEDGMENTS

The authors thank all of the participants in ICARTT/NEAQS 2004 who aided in the operation of these instruments and the collection of data. A special thanks goes to the dedicated officers and crew of the NOAA R/V Ronald H. Brown including our colleagues Sara Tucker, Janet Machol, Dan Law, and Rob Newsom for long hours collecting HRDL

data on ship. This work was supported by DOE, the NOAA Health of the Atmosphere program and the NOAA Earth System Research Laboratory.

REFERENCES

1. Kindler D., Oldroyd A., MacAskill A., and Finch D., An eight month test campaign of the Qinetiq ZephIR system: Preliminary results. *Meteor. Z*. 2007: **16**, 479–489.
2. Mann, J., Pen˜a A., Bingol F., Wagner R., and Courtney MS. Lidar scanning of momentum flux in and above the atmospheric surface layer. *J. Atmos. Oceanic Technol.* 2010*:* **27**, 959–976.
3. Pichugina YL and Banta RM. Stable boundary-layer depth from high-resolution measurements of the mean wind profile. *J. Appl. Meteor. Climatol*. 2010: **49**, 20-35.
4. Brewer WA, Tucker S C, Post MJ, Wolfe DE, Pichugina YL, Intrieri J. and Hardesty RM. Performance and results from recent ship-borne and ground-based boundary layer measurements using NOAA/ETL coherent Doppler lidars. *13th Coherent Laser Radar Conference*, 2005: Kamakura, Japan, **13,** 92-95.
5. Cañadillas B., Neumann T. First Test of a Nacelle-based “2-beam” Wind LiDAR System under Offshore Conditions, *DEWI MAGAZIN* 2011: **39**
6. Grund, CJ, Banta RM, George JL, Howell JN, Post MJ, Richter RA, Weickmann AM. High-resolution Doppler lidar for boundary layer and cloud research. *J. Atmos. Oceanic Tech*., 2001: **18**, pp 376-393.
7. Wulfmeyer VO, Randall M., Brewer WA, and Hardesty RM. 2 mm Doppler lidar transmitter with high frequency stability and low chirp. *Opt. Lett*. 2000: **25**, 1228-1230.
8. Pichugina Y L, Banta RM, Brewer WA, Sandberg SP, and Hardesty RM. Doppler-lidar-based wind-profile measurement system for offshore wind-energy and other marine-boundary-layer applications. *J. Appl. Meteor. Climatol*. 2012: **51**, 8, pp 327-349

9. Angevine WM, Hare JE, Fairall CW, Wolfe DE, Hill RJ, Brewer WA, and White B. Structure and formation of the highly stable marine boundary layer over the Gulf of Maine, *J. Geophys. Res*. 2006: **111**, D23S22, doi: 10.1029 / 2006JD007465.
10. Fairall CW, Ludovic B., Grachev AA, Hill RJ, Wolfe DE, Brewer WA, Tucker S., Hare JE, and Angevine W. Coastal effects on turbulent bulk transfer coefficients and ozone deposition velocity in ICARTT. *J. Geophys. Res*., 2006: **111**, D23S20, doi:1029/2006JD007597.
11. Wolfe DE, Brewer WA, Tucker SC, White AB, White DE, Welsh DC, Ruffieux D., Fairall CW, M. Ratterree M., Intrieri JM, McCarty BJ, and Law DC. Shipboard multi-sensor merged wind profiles from NEAQS 2004. *J. Geophys. Res.*, 2007: **112,** D10S15.
12. White AB, Darby LS, Senff CJ, King CW, Banta RM, Koermer J, Wilczak JM, Neiman PJ, Angevine WM, and Talbot R. Comparing the impact of meteorological variability on surface ozone during the NEAQS (2002) and ICARTT (2004) field campaigns. *J. Geophys. Res.* 2007: **112**, D10S14, doi:10.1029/2006JD007590.
13. Wagner R., Antoniou I., Pedersen SM, Courtney MS, Jørgensen HE. The influence of the wind speed profile on wind turbine performance measurements. *Wind Energy*, 2009: **12(**4), 348-362
14. Choukulkar A., Pichugina Y., Clack C., Calhoun R., Banta R., Brewer A., Hardesty M. A New Formulation for Equivalent Wind Speed and Power Calculations Using Data from the High Resolution Doppler Lidar. *Wind Energy*, 2015: accepted
15. Blackadar AK. Boundary layer wind maxima and their significance for the growth of nocturnal inversion. *Bull. Amer. Meteor. Soc*., 1957: **38**, 283–290.
16. Bonner WD. Climatology of the low level jet. *Mon. Wea.Rev.,* 1968: **96**, 833–850.
17. Parish T., Rodi AR, and Clark RD. A case study of the summertime Great Plains low level jet. *Mon. Wea. Rev.,* 1988: **116**, 94–105.

18. Banta RM, Newsom RK, Lundquist JK, Pichugina YP, Coulter RL, and Mahrt L., Nocturnal low-level jet characteristics over Kansas during CASES-99. *Boundary-Layer Meteorol*, 2002: **105**, 221-252.
19. Andreas EL, Claffey KJ, and. Makshtas AP. Low-level atmospheric jets and inversions over the western Weddell sea. *Bound.-Layer Meteor*., 2000: **97**, 459–486.
20. Kelley N. Shirazi M., Jager D., Wilde S., Adams J., Buhl M., Sullivan P., and Patton E. Lamar Low-Level Jet Project Interim Report. *NREL/TP-500-34593*. 2004: Golden, CO, National Renewable Energy Laboratory.
21. Kelley N., Jonkman B., Scott G. The Great Plains turbulence environment: its origins, impact and simulation. *Technical Report NREL/CP-50040176, National Renewable Energy Laboratory*, 2006.
22. Doyle J., Warner TA. Carolina coastal low-level jet during GALE IOP 2. *Monthly Weather Review* 2010: **138**, 2385–2404.
23. Jiang Q., Wang S., O'Neill L. Some insights into the characteristics and dynamics of the Chilean low-level coastal jet. *Monthly Weather Review*. 2010: **138**, 3185–3206.
24. Colle B., Novak D. The New York Bight jet: climatology and dynamical evolution. *Monthly Weather Review.* 2010: **138**, 2385–2404.
25. Zhang D., Zhang S., Weaver S. Low-level jets over the Mid-Atlantic states: a warm season climatology and a case study. *Journal of Applied Meteorology and Climatology.* 2006: **45,** 194–209.
26. Parish T. Forcing of the summertime low-level jet along the California coast. *J. Appl. Meteor.*, 2000: **39**, 2421–2433.
27. SgurrControl technical paper. Mitigating the Damaging Effects of Offshore Low Level Jets with Lidar and Individual Blade Control. *EWEA Offshore*. 2013: 19-21 November, Messe Frankfurt, Germany
28. Pichugina YL, Banta RM, Kelley ND, Jonkman BJ, Tucker SC, Newsom RK, and Brewer WA. Horizontal-Velocity and Variance Measurements in the Stable Boundary

Layer using Doppler Lidar: Sensitivity to Averaging Procedures, *J. Atmos. Ocean. Technol.* 2008: **25**, 1307-1327.

29. Banta RM, Pichugina YL, Kelley ND, Hardesty RM, Brewer WA. Wind energy meteorology: Insight into wind properties in the turbine-rotor layer of the atmosphere from high resolution Doppler lidar. *Bulletin of the American Meteorological Society*. 2013: **94**, 6, 883-902. doi: http://dx.doi.org/10.1175/BAMS-D-11-00057.1
30. Darby LS, McKeen SA, Senff CJ, White AB, Banta RM, Post MJ, Brewer WA, Marchbanks RD, Alvarez RD II, Peckham SE, Mao H., and Talbot R. Ozone differences between near-coastal and offshore sites in New England: Role of meteorology. *J. Geophys. Res*. 2007: **112**, D16S91, doi:10.1029/2007JD008446.
31. Stensrud D.J., 1996: Importance of low-level jets to climate: A review. *J. Climate*, **9**, 1698–1711
32. Banta RM, Pichugina YL, and Newsom RK. Relationship between low-level jet properties and turbulence kinetic energy in the nocturnal stable boundary layer. *J. Atmos. Sci*. 2003: 60, 2549–2555.
33. Banta RM, Pichugina YL and W.A. Brewer, 2006: Turbulent velocity-variance profiles in the stable boundary layer generated by a nocturnal low-level jet. *J. Atmos. Sci*., **63**, 2700-2719. 344
34. James, E., S. Benjamin, and M. Marquis, 2016: Offshore wind speed estimates from a high-resolution rapidly-updating numerical weather prediction model forecast dataset. Wind Energy, submitted.
35. DOE "Positioning of Offshore Wind Energy Resources (POWER), *DOE Report*, 2014, pp 146
36. Nunalee and Basu. Mesoscale modeling of coastal low-level jets: implications for offshore wind resource estimation. *Wind Energy.* 2014: **17**, 1199–1216

37. Sun J., Mahrt L., Banta RM, and Pichugina YL. Turbulence regimes and turbulence intermittency in the stable boundary layer during CASES-99. *J. Atmos. Sci.,* 2003: 69, 338–351.
38. Shaw et al., 2012, DOE "Offshore Resource Assessment and Design Conditions: A Data Requirements and Gaps Analysis for Offshore Renewable Energy Systems", *DOE*, 75 pp
39. DOE. A national offshore wind strategy creating an offshore wind energy industry in the United States. *Technical Report DOE/GO-102011 -2988*, *US Department of Energy,* 2011. 82.
40. Schreck S., Lundquist JK, and. Shaw W. U.S. Department of Energy Workshop Report - Research Needs for Wind Resource Characterization. *NREL Report No. TP-500-43521*. 2008: 116 pp.
41. Stewart, G. M.*,* Robertson, A.*,* Jonkman, J.*, and* Lackner, M. A. *(*2015*)* The creation of a comprehensive metocean data set for offshore wind turbine simulations*. Wind Energ., doi:* 10.1002/we.1881*.*
42. Smith K., Randall G., Malcolm D., Kelley N., Smith B. Evaluation of Wind Shear Patterns at Midwest Wind Energy Facilities. *Proceedings American Wind Energy Association (AWEA) Windpower Conference.* 2002:16 pp.
43. Pichugina YP, Banta RM, Kelley ND, and Brewer WA. Advancing wind energy research through new remote sensing technologies*. Proceedings, WINDPOWER 2007 conference*. 2007: June 3-6, Los Angeles, CA
44. Germanischer Lloyd, Rules for Classification and Construction, III Offshore Technology, 2 "Offshore Installations". Edition 1999
45. Antoniou I., Wagner R., Thomsen K., Paulsen U.,.Madsen HA, Pedersen SM, Jørgensen HE, Enevoldsen P., and Thesbjerg L. Influence of wind characteristics on turbine performance, *European Wind Energy Conference & Exhibition.* 2007*:* Milan, Italy, May 7-10.

46. Elliot DL and Cadogan JB. Effects of wind shear and turbulence on wind turbine power curves, *EWEC*. 1990: September 10–14, Madrid, Spain.
47. Akhmatov V. Influence of wind direction on intense power fluctuations in large offshore wind farms in the North Sea. *Wind Engineering*. 2007: **31**(1), 59-64.
48. Pedersen TF. On wind turbine power performance measurement at inclined airflow. *Wind Energy*. 2004: **7**, 163-176.
49. Pichugina YL, Banta RM, Brewer WA, Lundquist JK, Hardesty RM, Aitken ML, Alvarez RJ, Sandberg SP, Weickmann AM, Kelley ND, and Mirocha JD. Estimation of wind turbine wake characteristics. *Proceedings, 26th International Laser Radar Conference.* 2011: Porto Heli, Greece, pp 9-10
50. Banta, R.M., Y.L. Pichugina, W.A. Brewer, J.K. Lundquist, N.D. Kelley, S.P. Sandberg, R.J. Alvarez, R.M. Hardesty, A.M. Weickmann, 2015: 3-D volumetric analysis of wind-turbine wake properties in the atmosphere using high-resolution Doppler lidar. *J. Atmos. Oceanic Technol.*, **32**, 904-914, doi:10.1175/JTECH-D-00078.1.
51. Kaiser K., Langreder W., Hohlen H., Højstrup J. Turbulence correction for power curves. *Wind Energy.* 2007: 159-162.
52. Clack C., Alexander C., Choukulkar A., and MacDonald S. Demonstrating the effect of vertical and directional shear for resource mapping of wind power. *Wind Energy.* 2015: under Review.

Figure Captions

Figure 1. Google map image of ship tracks during the NEAQS-04 experiments. Each yellow dot represents an individual location of lidar measurements at a given time.

Figure 2. Left - Correlation coefficients between HRDL and radiosonde wind speeds up to 1500 m. Right - Number of points used in calculations at each height. Comparisons were made at rawinsonde launch times every 6 h for the entire NEAQS-04 dataset.

Figure 3. Time-height cross sections of HRDL-measured, 15-min averaged wind speed for August 11. Vertical axis is height above sea level (m), and horizontal axis is time, UTC (local Eastern Standard Time lags UTC by 5 h).

Figure 4. Selected 15-min-mean wind-speed profiles measured by HRDL on August 11. Red dots indicate LLJ maxima and horizontal dashed lines designate the heights of top and bottom of hypothetical turbine rotor-blade tips (50 and 150 m).

Figure 5. Distributions of jet speed U_J (top panel, m s^{-1}) and height (m) of the maximum speed Z_J (bottom panel) of the 15-min profiles of the NEAQS-04 HRDL dataset. Total number of occurrences in each bin is indicated along the left vertical axis, and percentages of occurrences in each bin are shown along right vertical axis. Red and blue lines in each distribution indicate mean and median values.

Figure 6a. Scatter plot of the HRDL-measured jet speed maxima (U_J) vs. the height of these maxima (Z_J). Black symbols indicate the tendency of stronger jets to occur at higher elevations. The color symbols indicate some periods when stronger U_J values were located at low levels close to hub-height.

Figure 6b. Time-height cross sections of 15-min wind speed (m s^{-1}) and direction (arrows), measured by HRDL on July 31, 2004. Horizontal lines show rotor layer of 50-150 m.

Figure 6c. Time-series of LLJ speed maxima (m s^{-1}, red symbols, right axis) and the height (m) of these maxima (blue symbols, left axis) for same dataset and the sample period in (b).

Figure 7. Spatial distribution of (a) LLJ speed maxima (m s^{-1}) and (b) height (m) of these maxima (ASL), based on 15-min HRDL-measured wind-profile data. Variables on both plots are scaled according to the color scale at the top of each plot.

Figure 8. Selected examples of wind-speed profiles obtained on August 8 illustrate (from left to right) positive, negative, and negligible net shear through the rotor layer. Profiles are 15-min HRDL wind-speed profiles taken at (a) 07/17/04 7:45 UTC; (b) 07/30/04 2:00 UTC, and (c) 07/31/04 1:00 UTC.

Figure 9. Figure 9. Time-series of HRDL-measured 15-min-mean wind (a) speed and (b) direction vs. hour of day, averaged over the entire NEAQS-04 experiment. Black lines in both panels show values at hub height (100 m), blue and red lines are for these values at the bottom (50 m) and top (150 m) heights of the rotor layer. Time-series of the mean (c) wind shear and (d) directional shear. Black lines in both panels show shear through the rotor layer (50-150 m). Blue and red lines show shear through the layer above (100-150 m) and below (50-100 m) the hub height respectively. Dashed black lines on both panels indicate 0.

Figure 10a. Time series of lidar-measured wind speeds vs. hour of day at heights of (red solid line) 10 m and (blue solid line) 100 m, averaged over the duration of the experiment. Points show time of measurements. Dotted lines indicate ± one standard deviation of data from mean values at (red) 10 m and (blue) 100 m.

Figure 10b. Time series of the shear exponent computed from lidar-measured hub-height winds and those at the reference height of 10 m. The shear exponent was first computed for each 15-min wind speed data, and then averaged over number of days (~30) in the experiment. Two dotted horizontal lines indicate the values of 0.07 and 0.1, commonly used to estimate hub-height winds by the simplified power-law relation. Dashed lines indicate mean value for the nighttime (0.19) and daytime (0.12) hours. Solid line shows mean value of 0.16 for the entire experiment.

Figure 10c. Spatial distribution of HRDL-measured winds at 10 m (left), and 100 m (right) ASL for the entire experiment. Wind speeds on both plots are scaled from 0 to 15 m s^{-1} as shown in the color scale.

Figure 11. (Left) Distributions and (right) color-coded spatial variability of the shear exponent computed by the power-law relationship using lidar measured wind speed at 10 and 100 m, shown for (a, a1) all profiles, (b, b1) for LLJ-profiles, and (c, c1) profiles with no LLJ shape. Red and blue lines on the left plots indicate the mean and median of each distribution. The y-axes are same as in Fig. 5. Dataset is for the entire NEAQS-04 experiment.

Figure 12. Top: time series of the normalized differences in power estimates between the hub-height (P_H) and the rotor equivalent (P_{eq}) wind speeds. Thin dotted lines indicate ± one standard-deviation spread across the mean values. Bottom: time series of root mean square error (RMSE) between P_{eq} *and* P_H.

Table 1. Values of minimum, maximum, mean, and standard deviations of wind speed, direction, speed shear, and directional shear for the levels or layers indicated, measured by HRDL and averaged over the entire NEAQS campaign.

Height (layer)	**Min value**	**Max value**	**Mean value**	**STD**
Wind speed (m s^{-1})				
150 m	5.41	10.23	7.425	1.21
100 m	5.21	9.25	7.165	1.01
50 m	5.12	8.11	6.685	0.80
10 m	4.15	6.56	5.225	0.52
Wind direction (°)				
150 m	149.25	265.59	217.41	26.57
100 m	172.25	265.65	216.23	23.33
50 m	151.24	258.04	207.84	24.04
10 m	161.53	249.50	201.22	21.50
Wind speed shear (m s^{-1})				
50-150 m layer	-0.960472	1.78	0.78	0.53
100-150 m layer	-0.153866	0.93	0.29	0.26
50-100 m layer	-0.768758	1.16	0.52	0.34
10-100 m layer	-1.14768	3.25	1.96	0.74
Wind direction shear (°)				

50-150 m layer	-15.0685	36.75	10.49	10.13
100-150 m layer	-16.3454	26.135	4.19	8.27
50-100 m layer	-14.7416	46.725	7.73	9.51
10-100 m layer	-16.899	70.015	15.00	14.65

WE_2075_F1.tif

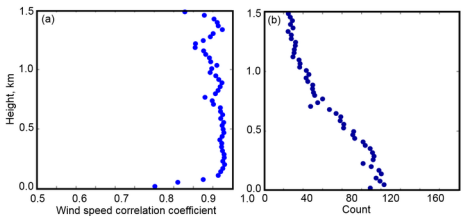

WE_2075_F2.tif

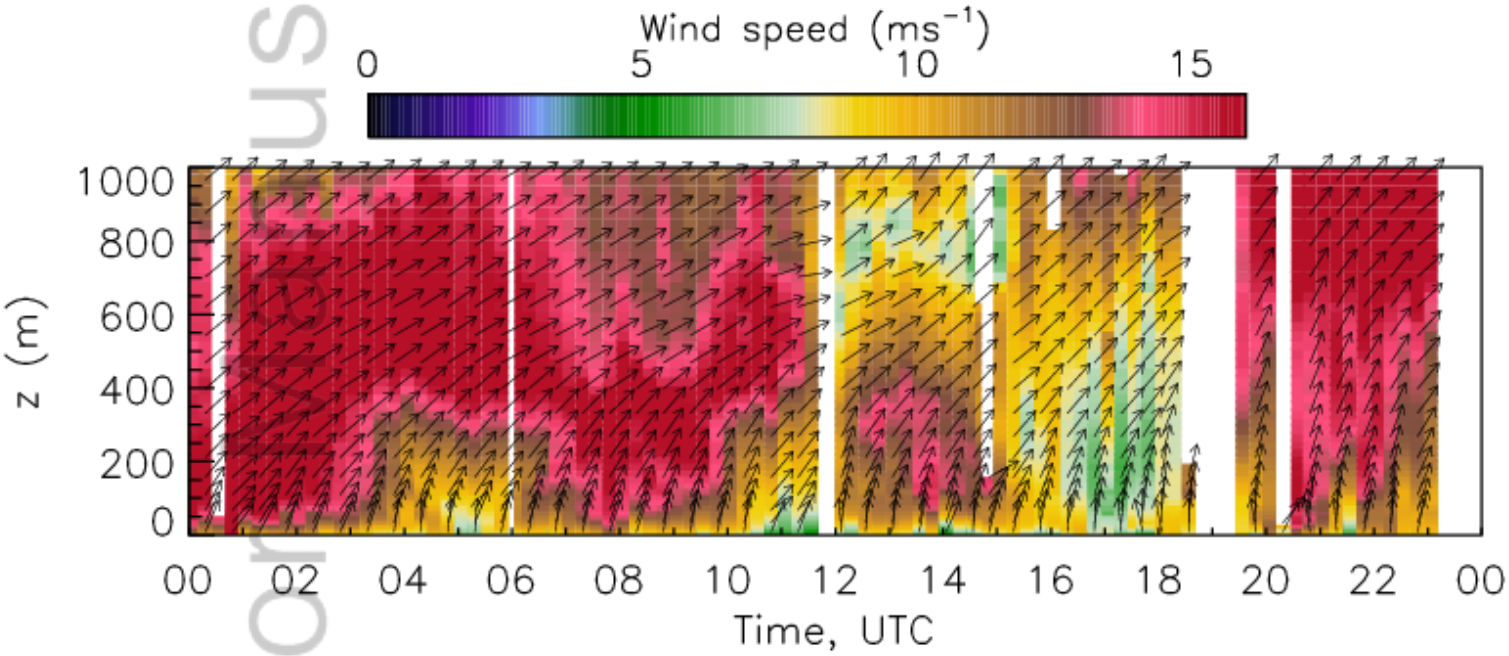

WE_2075_F3.tif

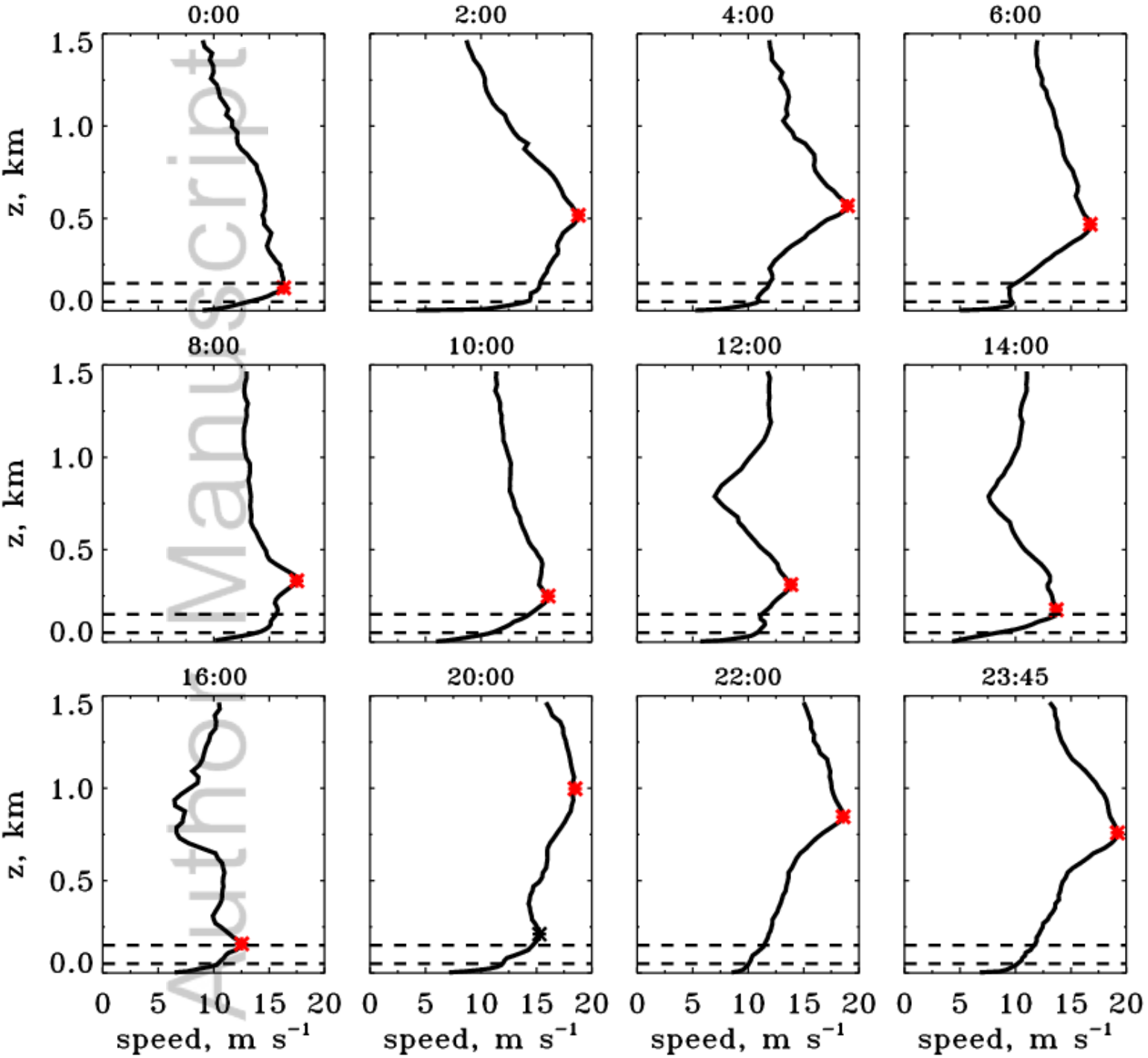

WE_2075_F4.tif

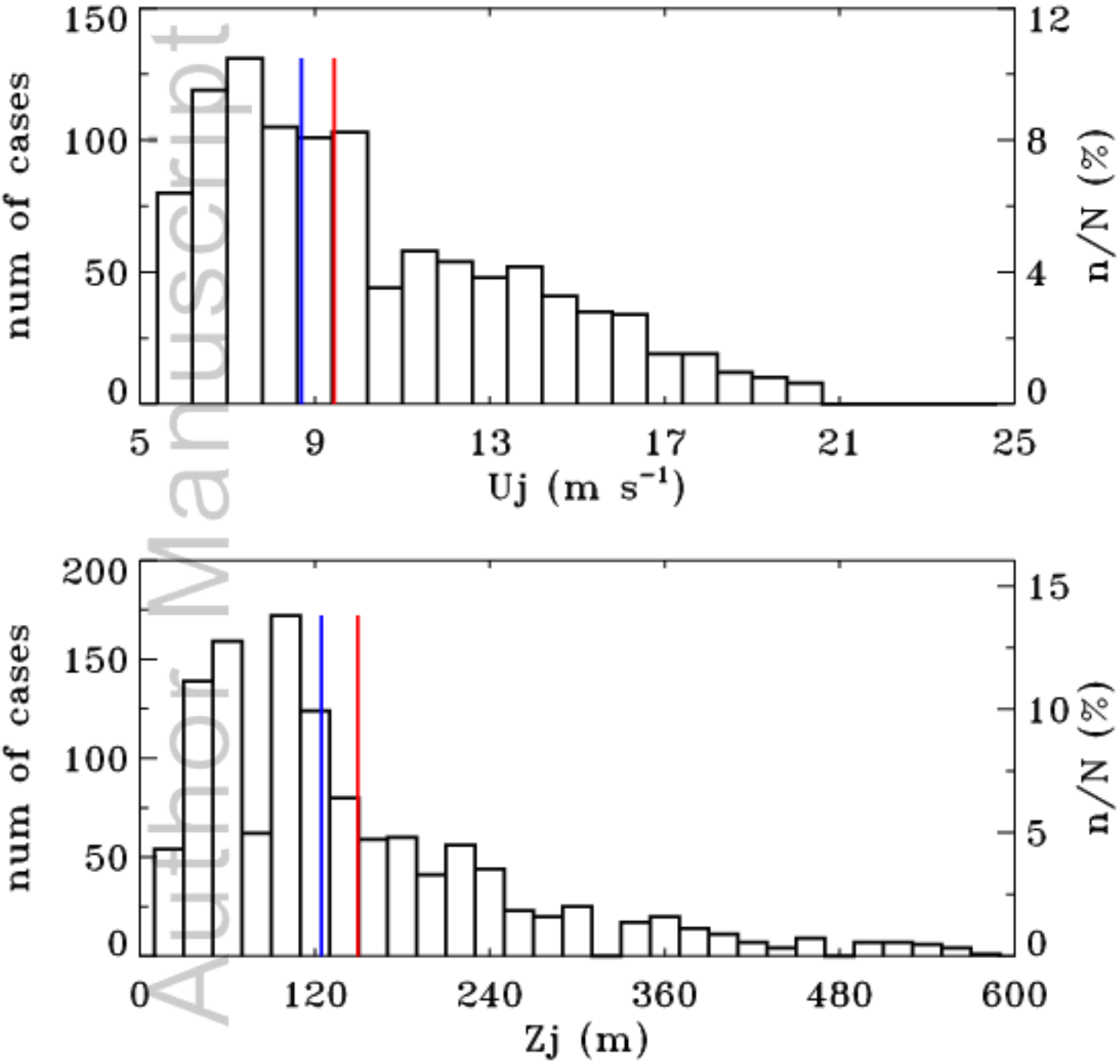

WE_2075_F5.tif

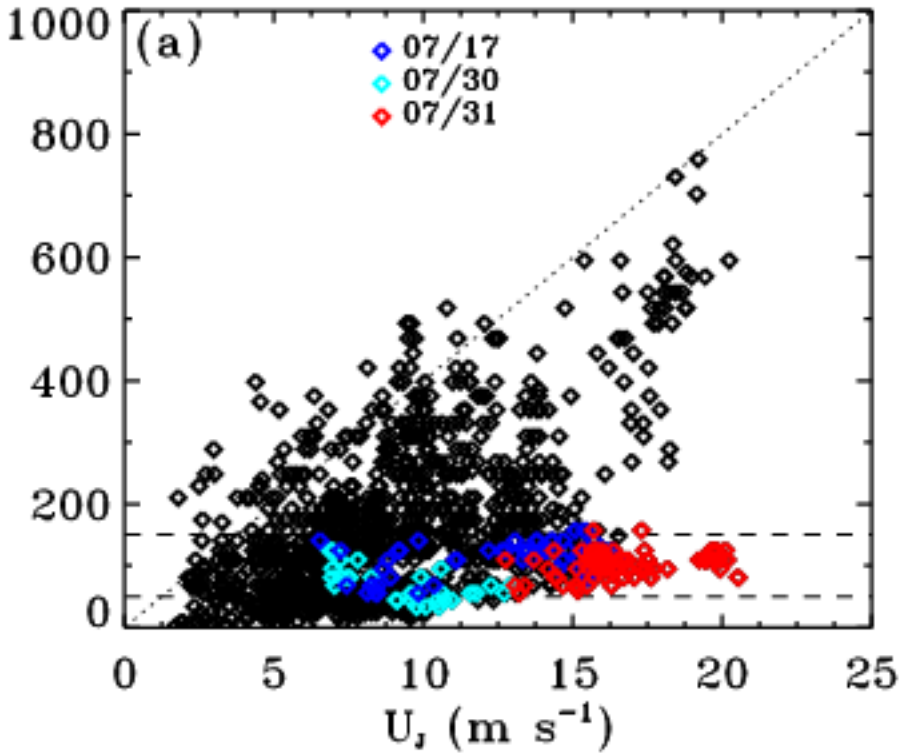

WE_2075_F6a.tif

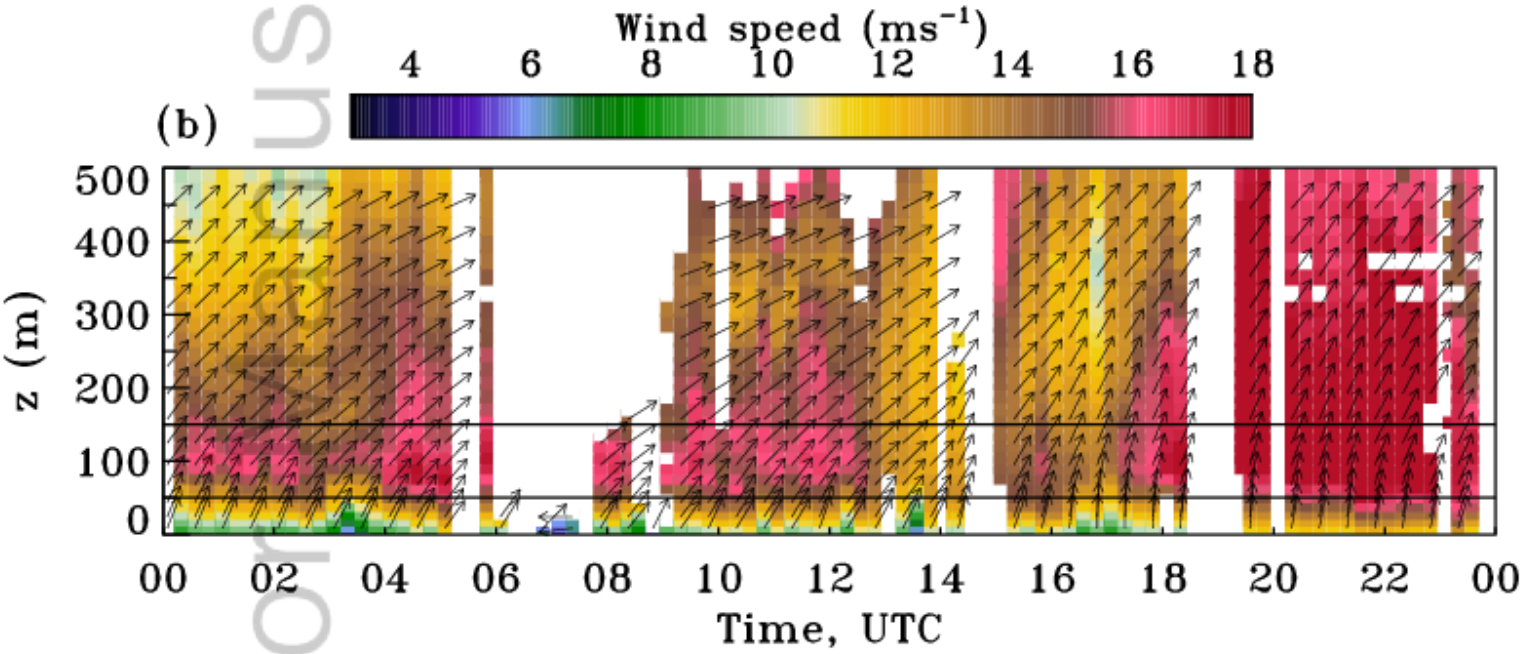

WE_2075_F6b.tif

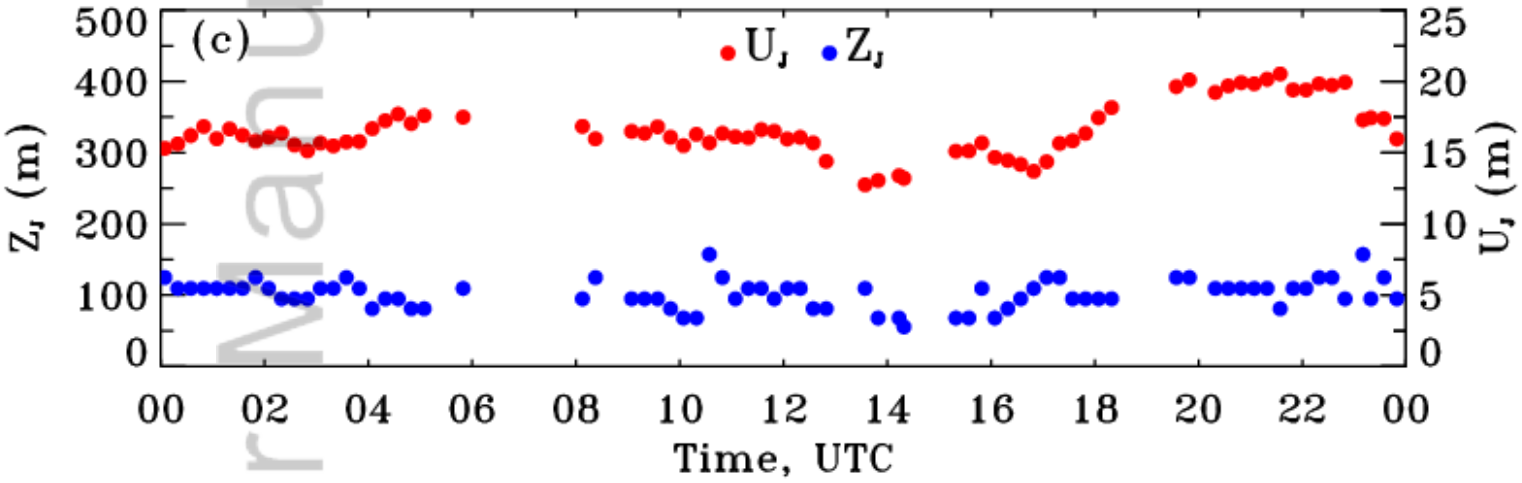

WE_2075_F6c.tif

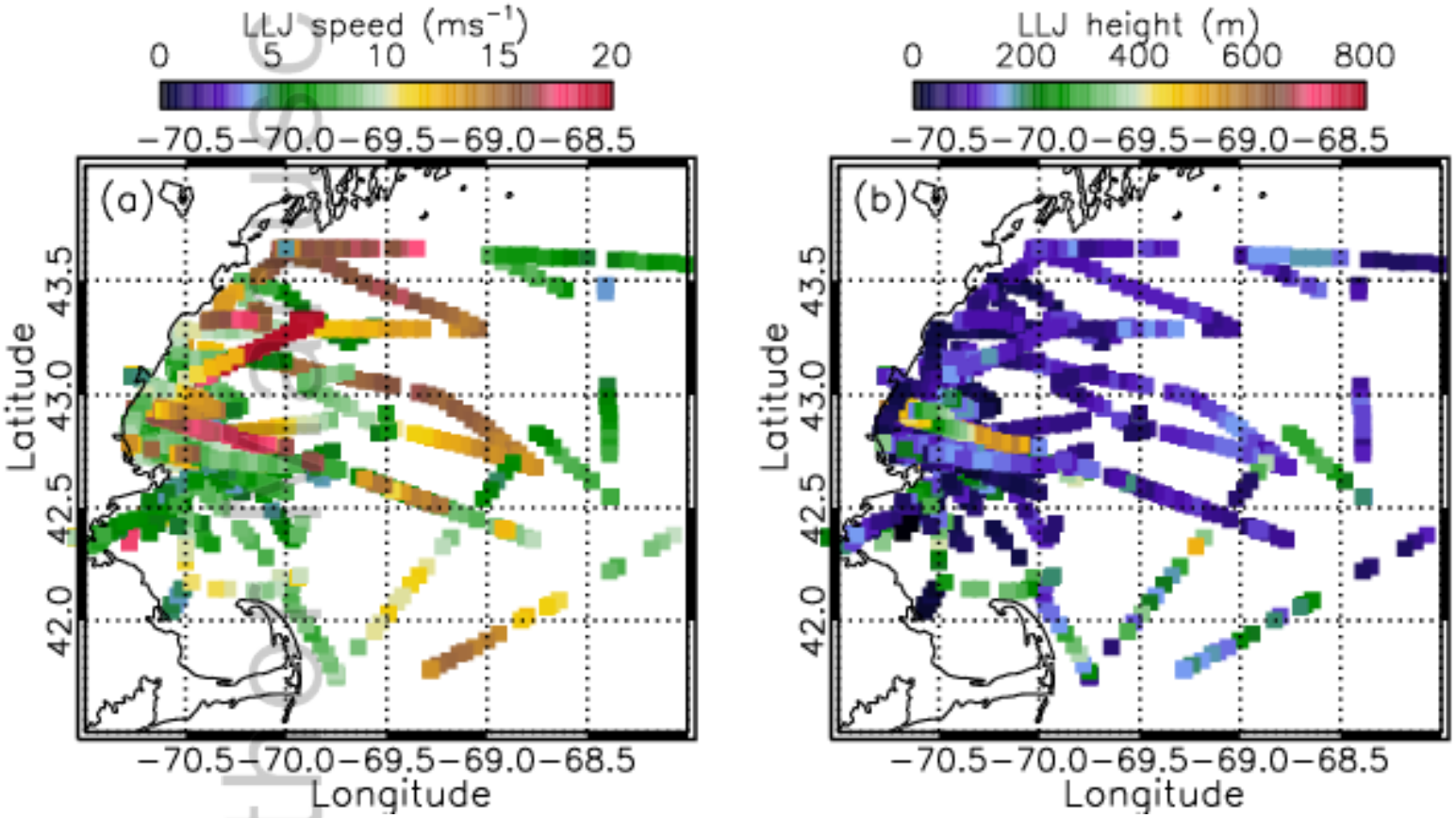

WE_2075_F7.tif

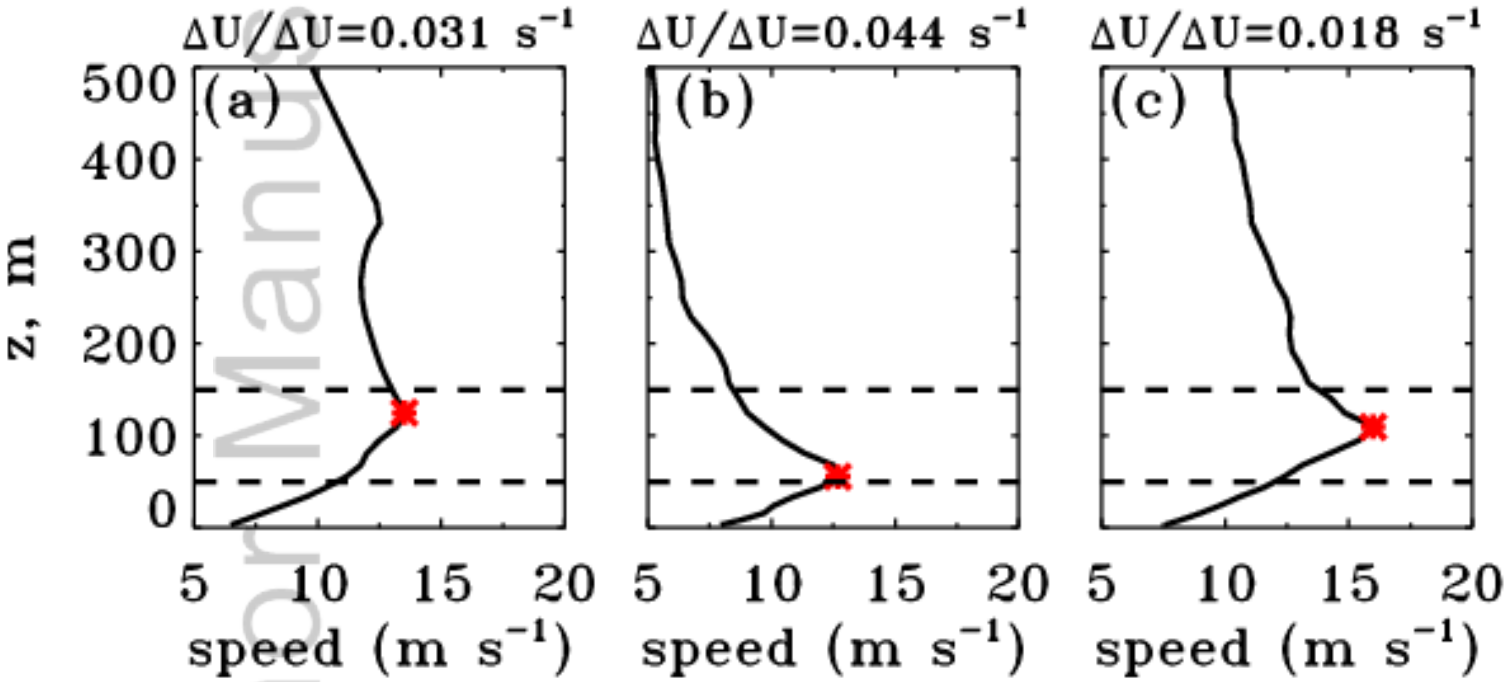

WE_2075_F8.tif

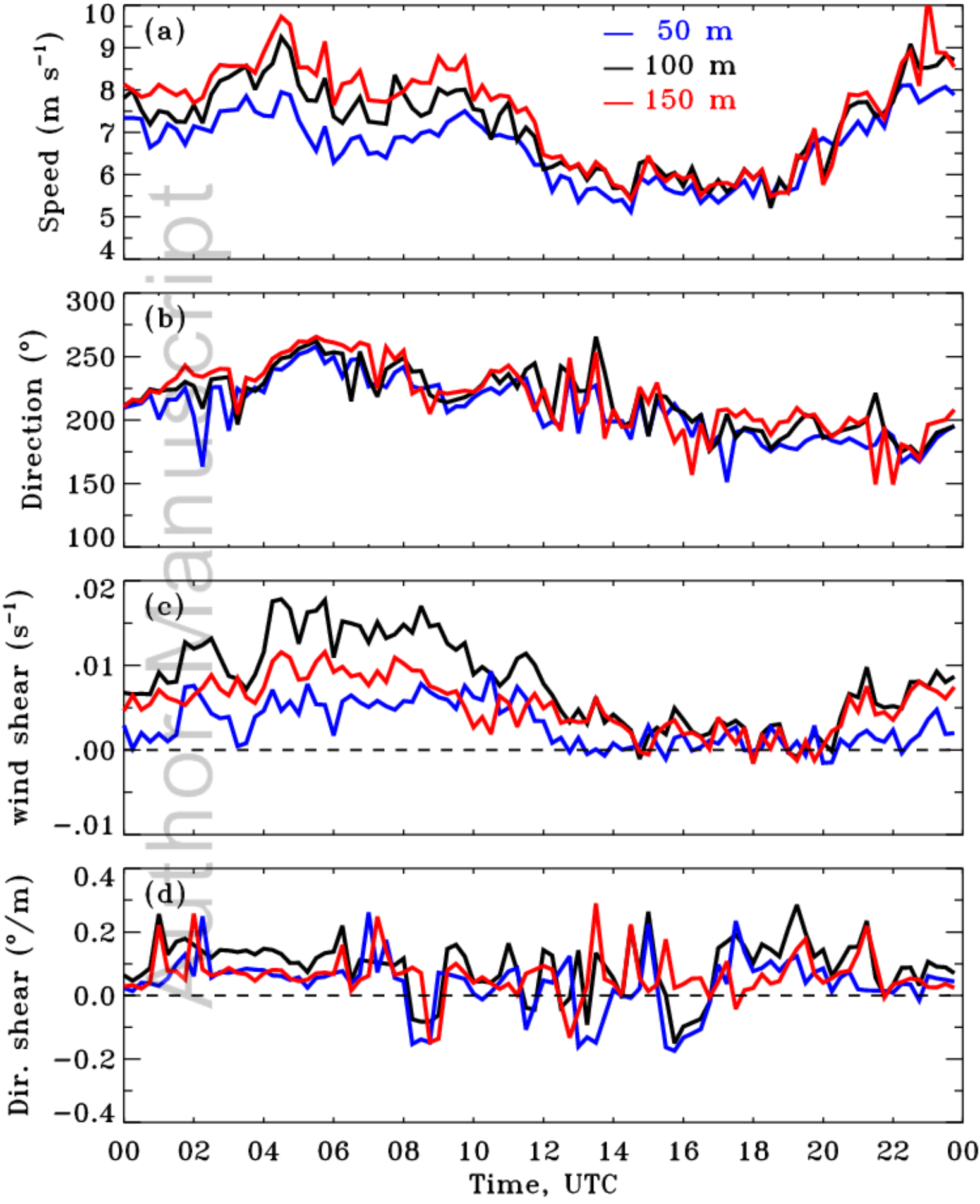

WE_2075_F9.tif

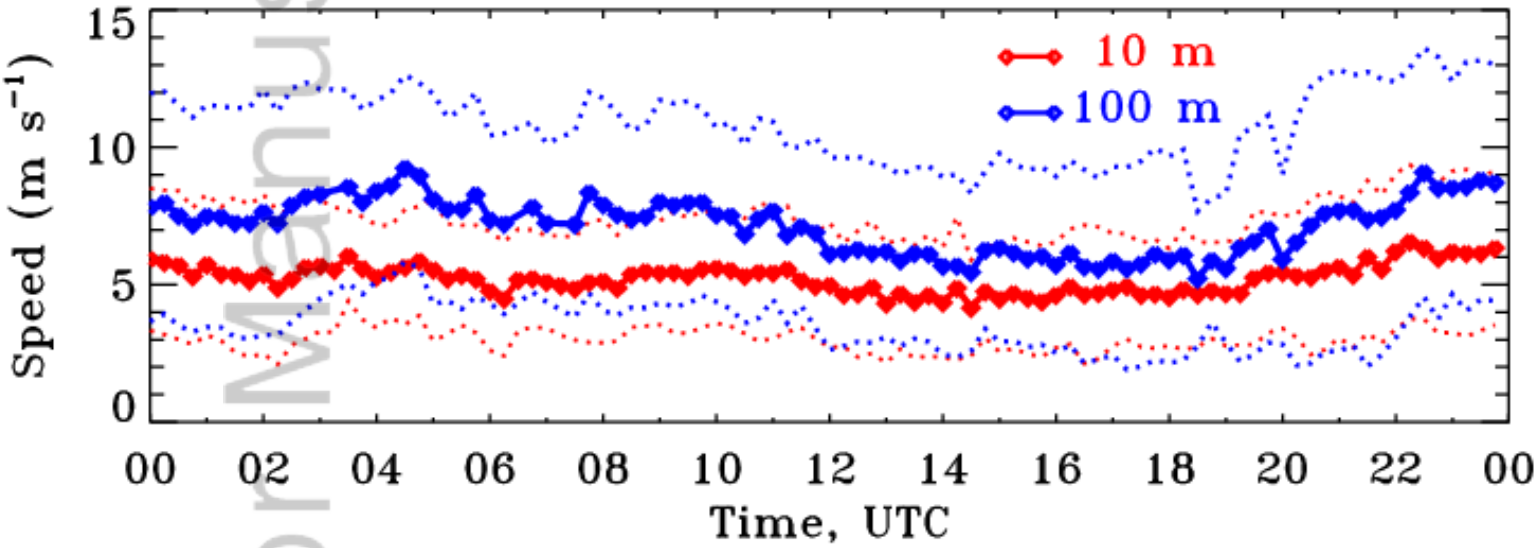

WE_2075_F10a.tif

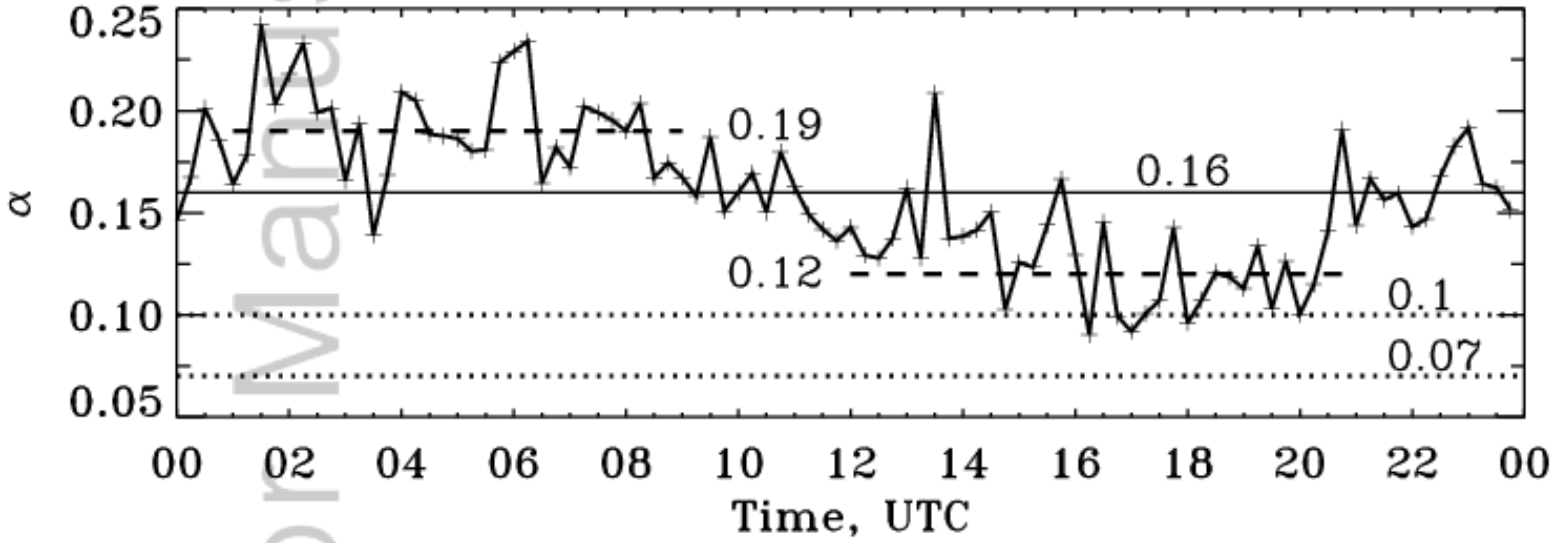

WE_2075_F10b.tif

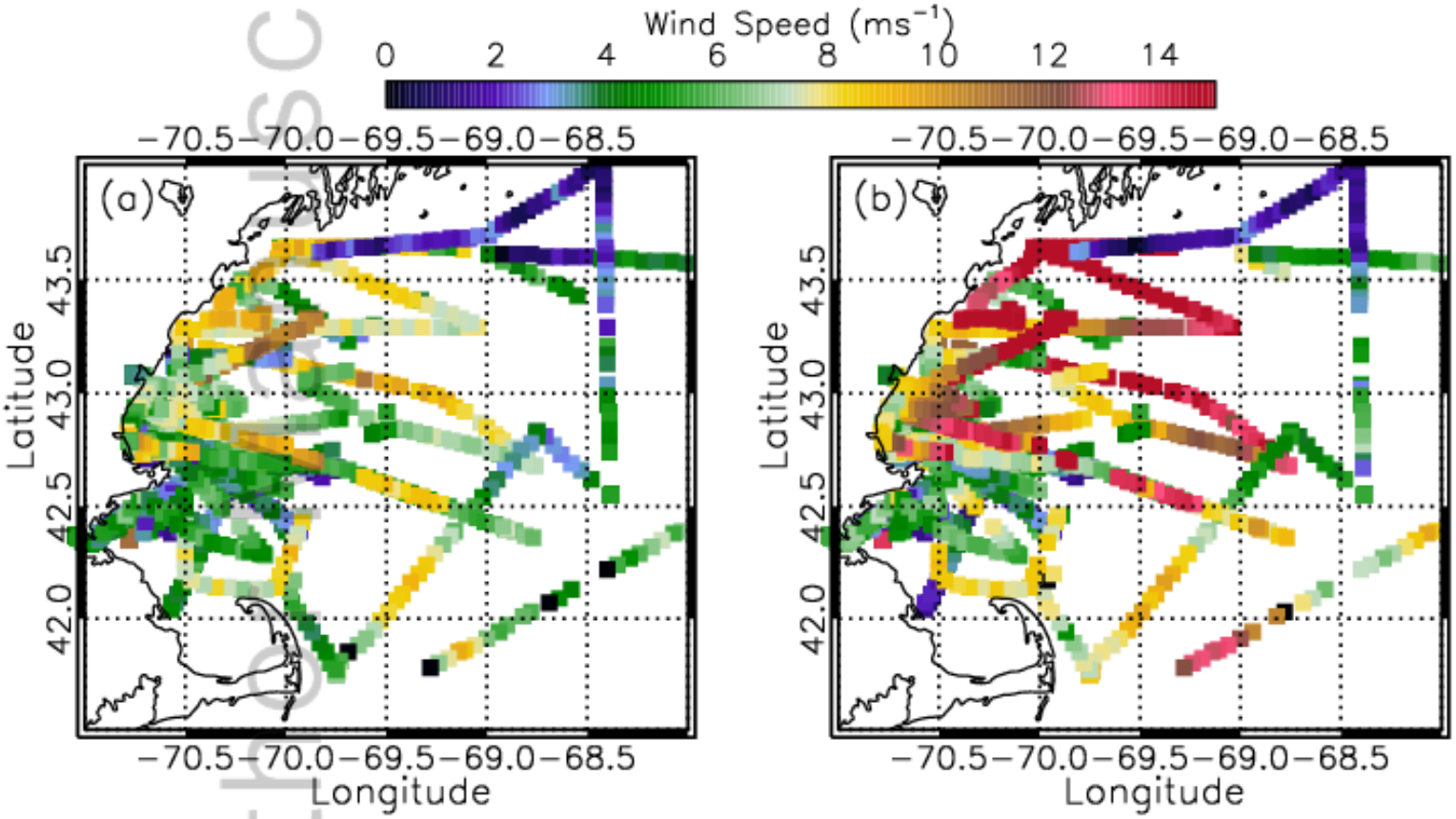

WE_2075_F10c.tif

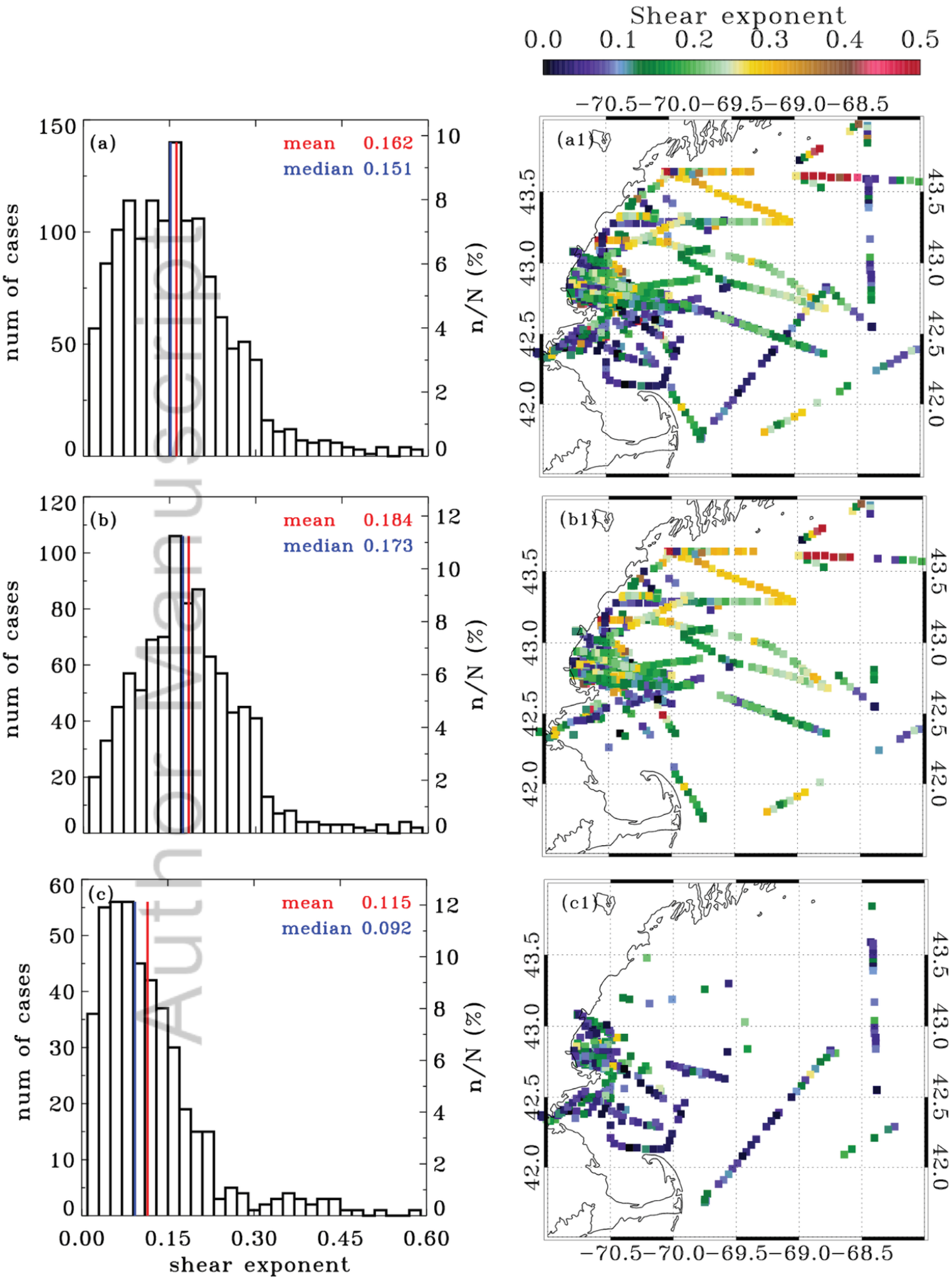

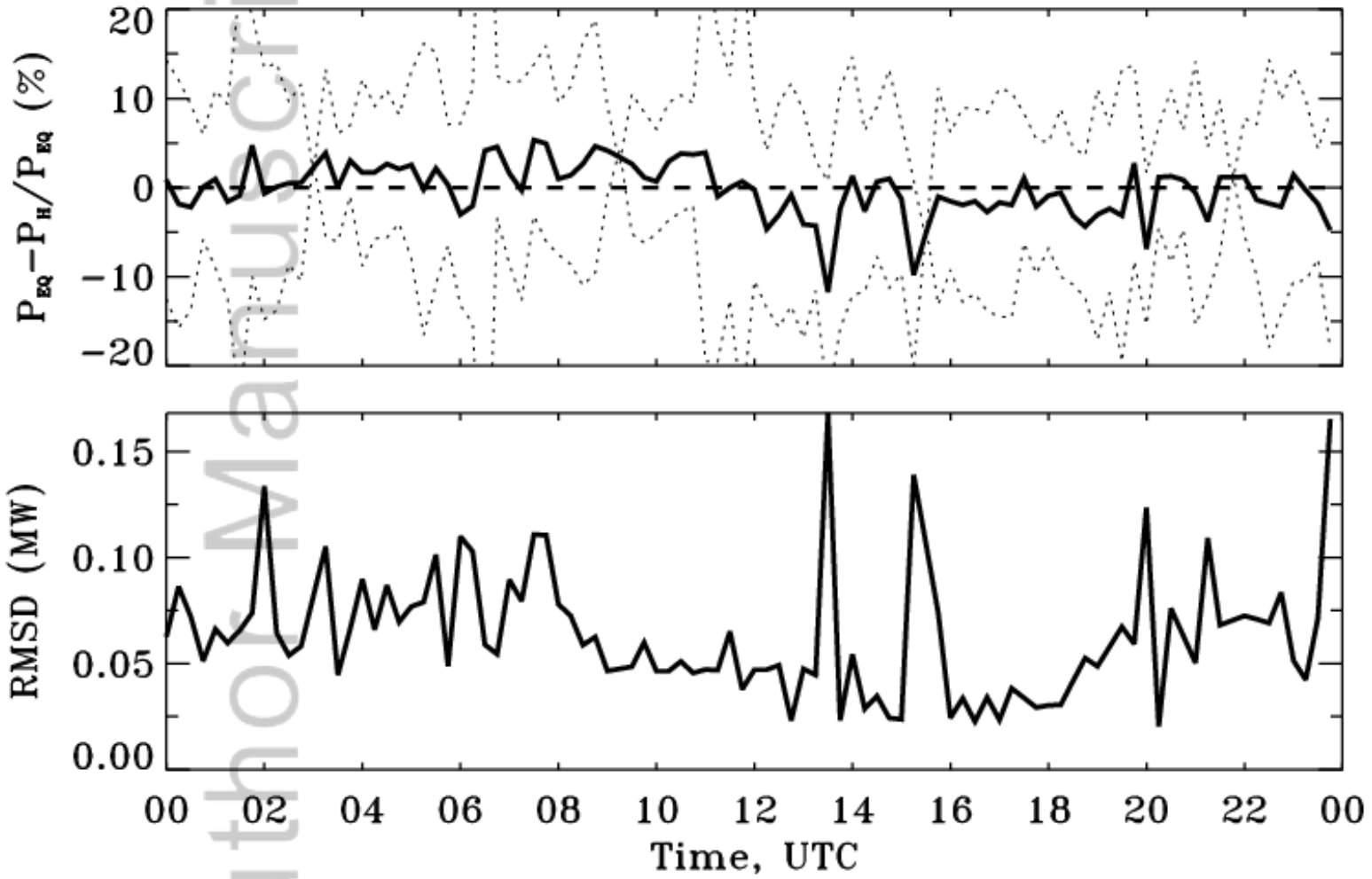

WE_2075_F12.tif